RSC Advances

PAPER

View Article Online
View Journal | View Issue

Cite this: *RSC Adv.*, 2025, **15**, 16597

Ion-modulated graphene oxide and GO@MXene hydrogels: enhanced adsorption performance and stability for methylene blue removal†

Xiaojing Chen,‡[ab] Jia Li,‡[a] Caojie Zhao,[a] Wen Zhou,[a] Jin Yang,[ab] Qingjun Liu *[a] and Wenshuai Jiang *[abc]

Ion cross-linking is often used to prepare graphene hydrogels, but the effects of different ion introductions on the properties of graphene hydrogels need to be further explored. In this study, graphene oxide (GO) and GO@MXene non-spherical hydrogels were prepared by introducing different ions, and their adsorption effects on methylene blue (MB) were discussed to determine their feasibility in water treatment. The adsorption efficiencies were significantly variable because the introduction of different ions had different effects on the internal structure and molding process of the hydrogels. The GO and GO@MXene hydrogels crosslinked with Ca^{2+} demonstrated superior MB adsorption performance compared to those prepared with K^{+} and Al^{3+}, achieving 85.2% and 85.8% MB removal efficiencies within 9 hours, respectively. Interestingly, the morphology of the hydrogel can be changed by adjusting the drop height, which in turn affects the MB adsorption. The results showed that hydrogels had faster MB removal by preparing them from a higher height (3.5 cm). The results demonstrated that hydrogels prepared from a higher droplet fall height (3.5 cm) exhibited accelerated MB removal, with a 10–20% enhancement in removal efficiency. In addition, the effects of pH and contact time on the adsorption performance of the hydrogels were investigated. The results showed that the best removal effect was achieved under neutral conditions, and the adsorption process was consistent with the pseudo-quadratic kinetic model (R^2 > 0.97). In addition, we found that the introduction of MXene enhanced the water stability of the hydrogels, which increased with the metal ion valence number. Furthermore, our study demonstrated that Ca^{2+}-crosslinked GO and GO@MXene hydrogels exhibit excellent selective adsorption of cationic dyes, achieving MB removal efficiencies of 96.6% and 98.3% in mixed dye systems, respectively. This study not only confirms that the introduction of ions can affect the properties of hydrogels by modulating their morphology, but also provides potential candidates for MB adsorption.

Received 8th April 2025
Accepted 13th May 2025

DOI: 10.1039/d5ra02422f

rsc.li/rsc-advances

1. Introduction

A hydrogel is a polymer system with a three-dimensional network structure containing a large amount of water formed by a simple reaction of one or more monomers.[1–5] In recent years, GO, as a two-dimensional carbon nanomaterial, has received extensive attention from the scientific community for its unique structure and properties.[6–9] GO hydrogel is a three-dimensional structure composed of GO cross-linked by self-assembly.[10–12] Attributed to the excellent physical, chemical, mechanical properties, abundant oxygen-containing functional groups, and good water dispersibility, GO hydrogels have been widely used in the fields of wastewater treatment,[13,14] catalysis,[15–17] biomedical applications,[18–20] energy storage devices,[21,22] supercapacitors[23,24] and sensors.[25,26]

To meet the needs of these applications, the assembly of GO into three-dimensional gel-like networks is the main issue that should be considered. Commonly used methods and strategies for the preparation of GO hydrogels are chemical modification, grafting GO, and acidification or addition of organic molecules, polymers, or ions as cross-linking agents, which can cross-link them through covalent and supramolecular interactions such as hydrogen bonding, ligand interactions, and hydrophobic interactions.[27–29] Among the previously reported hydrogels prepared by ionic cross-linking, divalent cation (Ca^{2+}, Mg^{2+} and Cu^{2+}) solutions were mostly used as cross-linking agents,[30–32] and other ion-modulated preparations of GO hydrogels have been rarely reported to the best of our knowledge. In addition to

[a]School of Medical Engineering, Xinxiang Medical University, Xinxiang, Henan 453003, People's Republic of China. E-mail: 171024@xxmu.edu.cn; qjliu@zju.edu.cn
[b]Xinxiang Key Laboratory of Neurobiosensor, Xinxiang, Henan 453003, People's Republic of China
[c]Henan Engineering Technology Research Center of Neural Sensing and Control, Henan 453003, People's Republic of China

† Electronic supplementary information (ESI) available. See DOI: https://doi.org/10.1039/d5ra02422f

‡ These authors contributed equally to this work.

this, our previous study showed that the introduction of different ions alters the electrical, luminescence and microwave radiation properties of GO membranes.[33] Therefore, it is necessary to investigate the effects of different ion introductions on the preparation of GO hydrogels and their properties.

In recent years, materials for the removal of organic dye molecules have been extensively explored.[34,35] Among these, MXene, which possesses excellent electrical, mechanical, chemical, and thermal properties,[36] has found extensive applications in various fields including energy storage, optoelectronics, biomedical engineering, communications, and environmental remediation. Since its discovery, MXene has been recognized as a potential adsorbent material. The surface of MXene is rich in functional groups (*e.g.*, –OH, –F, –O),[37,38] which can interact with dye molecules through both physical adsorption (van der Waals forces) and chemical adsorption mechanisms (such as hydrogen bonding and acid–base reactions). This gives MXene strong affinity for dye molecules and enables effective adsorption of various dyes.

In this study, we investigated GO and GO@MXene hydrogels regulated by different ions and found that the introduction of different ions affects their stability in water and adsorption of MB. Among them, Ca^{2+}-crosslinked hydrogels showed the best adsorption of MB. The kinetic results showed that the adsorption of MB conformed to the pseudo-secondary kinetic model. In addition, the height of the droplets falling into different ionic solutions affects the morphology of the prepared hydrogels, which in turn affects the adsorption of MB. Furthermore, Ca^{2+} cross-linked hydrogels were used for selective adsorption experiments to verify their feasibility in practical applications.

2. Materials and methods

2.1. Materials

GO solution (5 mg mL^{-1}) was purchased from Angxing New Carbon Materials Co., Ti_3C_2 (MXene, 5 mg mL^{-1}) was purchased from Beike 2D Materials Co. Ltd; MB was purchased from Tianjin Yongda Chemical Reagent Co. Ltd; methyl orange (MO) was purchased from Shanghai Aladdin Biochemical Technology Co.; sodium chloride (NaCl), potassium chloride (KCl) and calcium chloride ($CaCl_2$) were purchased from Tianjin Damao Chemical Reagent Factory, aluminum sulfate ($Al_2(SO_4)_3$) was purchased from Shanghai Eon Chemical Technology Co. Ltd; all chemicals and materials were not subjected to any additional purification, and ultrapure water was used for all experiments.

2.2. Preparation of GO and GO@MXene hydrogels

GO hydrogels were prepared using the cationic cross-linking technique. Briefly, the GO solution was continuously dripped into the salt solution (saturated KCl solution, 2% $CaCl_2$ solution, 4% $Al_2(SO_4)_3$ solution) by slowly pushing the syringe, and the formed GO hydrogels were placed in the salt solution for 1 hour to complete the cross-linking. After that, they were washed five times with ultrapure water for further use. With the mouth of the tube 0.5 cm away from the surface of the liquid. The GO hydrogels prepared by different ion cross-linking were named GO-M (M: Na, K, Ca, Al). The GO hydrogels prepared at different heights (0.5 cm and 3.5 cm) were named GO-M-L and GO-M-H, respectively.

Similarly, a mixed solution of GO with MXene ($V_{MXene} : V_{GO} = 1 : 4$) was used to prepare GO@MXene hydrogels through the same method. The GO@MXene hydrogels prepared by different

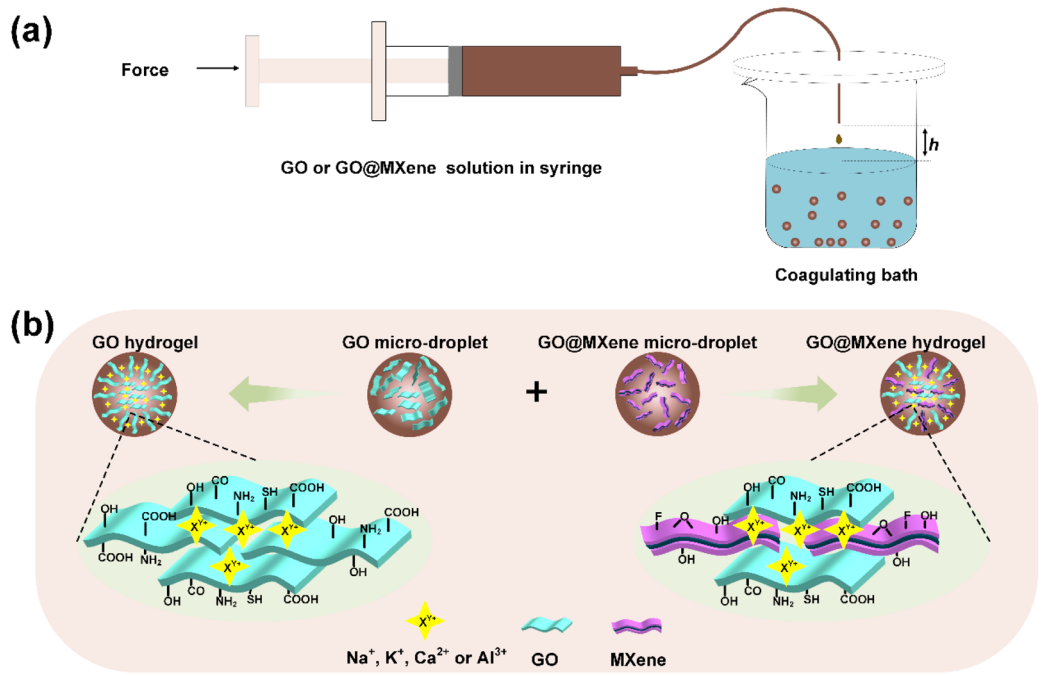

Fig. 1 Schematic of the preparation of GO and GO@MXene hydrogels (a). Self-assembly diagram of GO and GO@MXene hydrogels (b).

ion cross-linking were named GO@MXene (M: Na, K, Ca, Al). The GO@MXene hydrogels prepared at different heights (0.5 cm and 3.5 cm) were named GO@MXene-M-L and GO@MXene-M-H, respectively.

2.3. Characterization

Ultraviolet-visible Spectrophotometer (UV-vis, TU-1810 PC, China) was used to investigate the change in the absorbance of MB before and after adsorption. The microstructures of GO and GO@MXene hydrogels were characterized by field emission scanning electron microscope (SEM, Hitachi SU5000, Japan), and the elemental species of the hydrogels were analyzed by energy dispersive spectrometer (EDS, FEI TeN-Cai G2 f20 s-twin, 200 kV, USA). In addition, the X-ray photoelectron spectroscopy (XPS) results were obtained using a Thermo Fisher K-alpha spectrometer (EscaLab 250Xi, USA). Finally, the specific surface area and pore size of the hydrogels were measured using a specific surface and porosity analyzer (Micromeritics 3Flex, USA).

Fig. 1a illustrates the preparation process of GO and GO@MXene hydrogels. In this study, 2 mL of GO solution is first sucked into the syringe; subsequently, the GO solution is dripped continuously into the salt solution (NaCl, KCl, $CaCl_2$ and $Al_2(SO_4)_3$) by slowly pushing the syringe. When the droplets fall into the solution, GO-M hydrogels are obtained under the action of metal cations; finally, the prepared GO-M hydrogels was flushed by ultrawater in order to remove excess metal ions. Fig. 1b shows the cross-linking plot of GO and GO@MXene droplet assembly. Similarly, GO@MXene-M hydrogels can also be prepared by this method. In the pre-experiments, since GO-Na hydrogels underwent decomposition due to prolonged immersion in pure water, we focus on GO-M hydrogels modulated by potassium, calcium and aluminium ions.

3. Results and discussion

3.1. Characterisation

SEM was used to investigate the morphology of GO-M hydrogels, as shown in Fig. 2. According to Fig. 2a–c, the surface of GO-M hydrogels showed a non-homogeneous texture structure, implying an increase in surface roughness. The interior of the GO-M hydrogel exhibits an irregular porous structure (Fig. 2d–f). Besides, the SEM results in Fig. 2 also showed the morphology of the prepared hydrogels surfaces varied as a result of the introduction of different metal ions. The EDS mapping results in Fig. 2g–i also showed the distribution of different K, Ca, Al and O elements in GO-M hydrogels, indicating the successful preparation of GO-M hydrogels.

XPS of the GO-M hydrogels was performed to study their chemical states and compositions. As shown in Fig. 3a, the XPS survey spectra of GO-M indicate the presence of C and O. The corresponding GO hydrogels also contained K, Ca, and Al because of the different cross-linking cations. These results indicate the successful preparation of the GO-M hydrogels.

Fig. 3b–d show the nitrogen adsorption–desorption curves of the ion-crosslinked GO-M hydrogels. The analysis reveals that the isotherms of the GO hydrogels belong to Type IV with an H3-type hysteresis loop in the medium-to-high pressure region, indicating the presence of a mesoporous structure. From Fig. 3b–d it can be seen that the energy required for desorption is higher than that required for adsorption for all three samples. Comparing Fig. 3b–d, it can be seen that the difference in N_2 adsorption of GO-M at higher relative air pressure is not large,

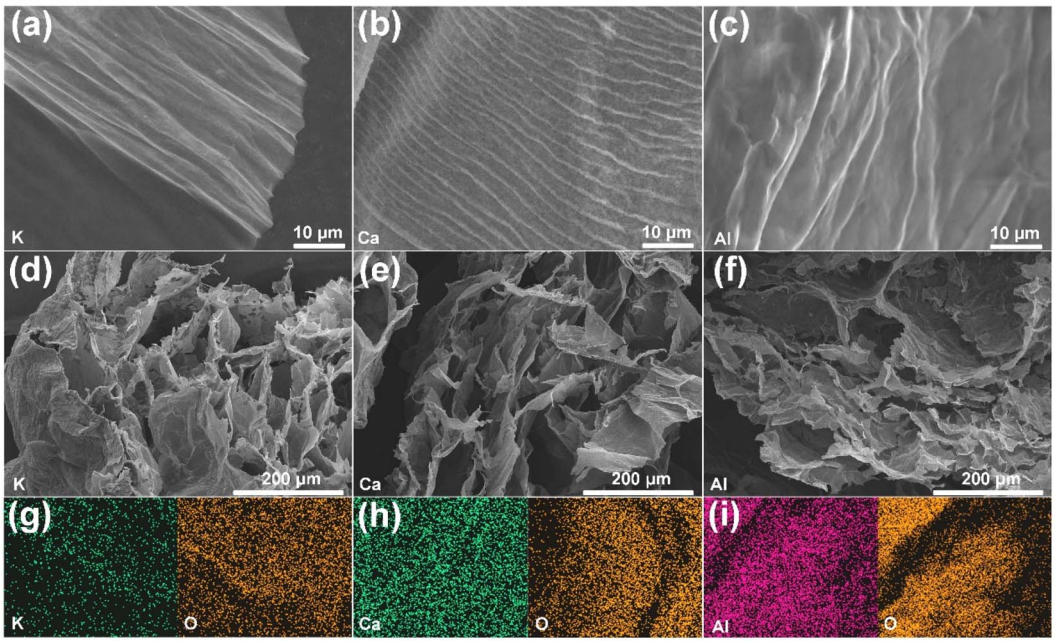

Fig. 2 SEM images of the surface (a–c) and cross-sectional (d–f) morphology of the GO-M hydrogel. (g–i) EDS results of GO-M hydrogels (M: K, Ca, Al).

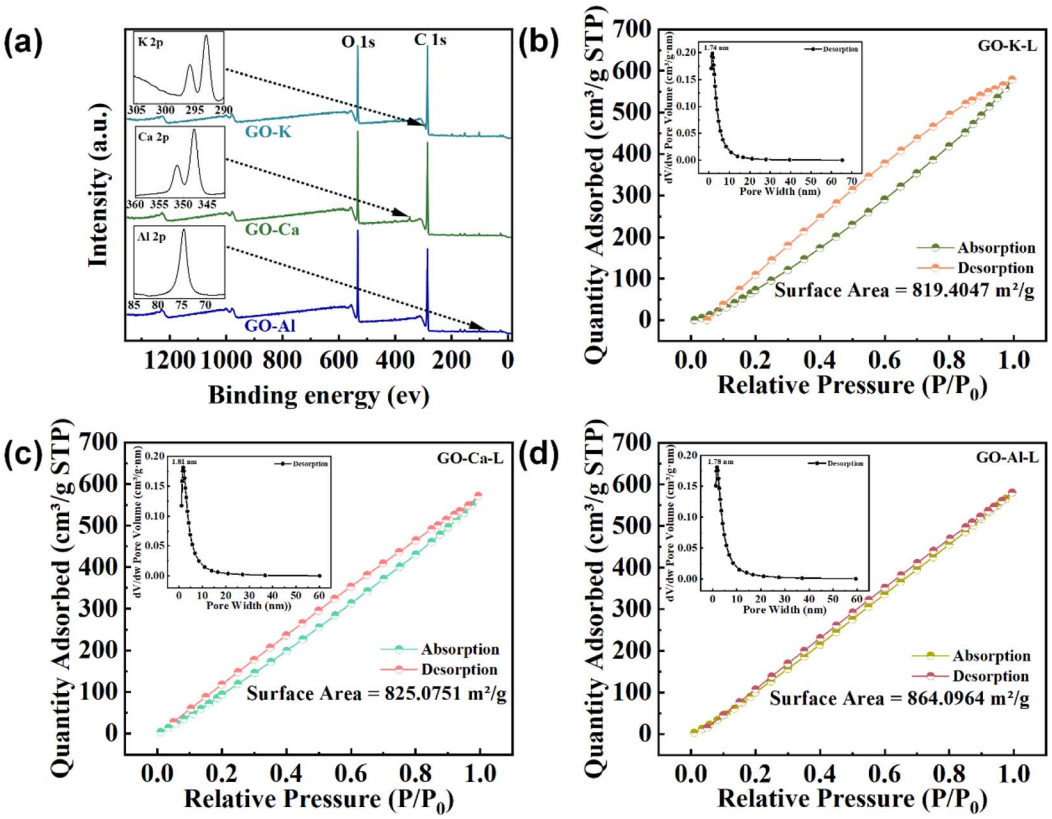

Fig. 3 XPS results of GO-M (a). Nitrogen adsorption and desorption profiles of ion-crosslinked GO-M hydrogels (b–d).

indicating that the difference in specific surface area is not significant (Table 1). From the pore size distribution, it can be seen that the pore size distributions of GO-M samples are all concentrated in 2–10 nm, and all of them show mesoporous structure, and have smaller pore size distributions and uniform pore structures. The high specific surface area (>800 $m^2\ g^{-1}$) and uniform pore size distribution provide abundant active sites, which are more favorable for MB adsorption, while the open pore structure facilitates rapid diffusion, consistent with the pseudo-second-order kinetic model.

3.2. Effect of droplet falling height on GO-M

Further, the shapes of GO-M samples prepared in this study were also affected by the droplet drop height and the ionic species in the solution (Fig. 4b). As shown in Fig. 4a, it was found that the shapes of GO-M-L samples prepared in different solutions were bullet-shaped when the droplet falling height was 0.5 cm. However, when the droplet falling height was 3.5 cm, the shape of the prepared GO-M-H samples was jellyfish-like in KCl solution and the shape of the prepared GO-M-H samples was cap-like in $CaCl_2$ and $Al_2(SO_4)_3$ solutions (Fig. 4a). The results indicate the shapes of the prepared GO-M can be regulated by adjusting the height and the type of metal ions in the solution.

Table 1 Pore structure analysis

Sample	BET ($m^2\ g^{-1}$)	Pore volume ($cm^3\ g^{-1}$)	Pore diameter (nm)
GO-K-L	819.4074	0.890888	3.2557
GO-Ca-L	825.0751	0.879001	3.3545
GO-Al-L	864.0964	0.894537	3.5718
GO-Ca-H	833.7923	0.923487	3.2436

3.3. MB adsorption based on GO-M

Considering the excellent performance of GO in MB removal,[39] it was hypothesized that changes in morphology and shape may affect the adsorption performance of GO-M. In addition, our previous studies have shown that the introduction of alkali and alkaline earth metal ions also alters the electrical, luminescence and microwave reduction properties of GO membranes.[33] Based on this, the effectiveness of methyl bromide removal based on GO-M was investigated, and the results were showed in Fig. 5. In this study, 2 mL GO solution was used to prepare GO-M; subsequently, the prepared samples were added into 20 mL MB solution with the concentration of 50 mg L^{-1} for investigating the removal of MB. The whole process was carried out at ambient temperature for a certain period. The change of MB concentration was determined by an UV-vis spectrophotometer. The removal rate was calculated using eqn (1):[40]

$$R\% = 100\% \times \frac{C_0 - C_t}{C_0} \quad (1)$$

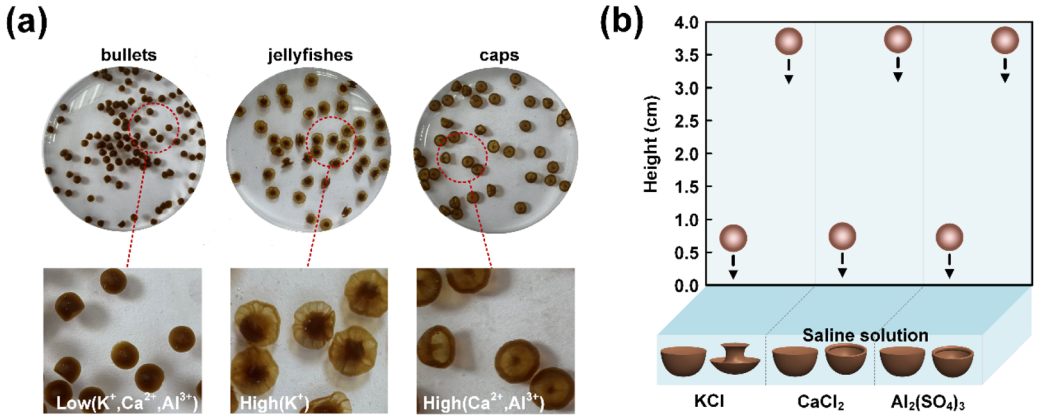

Fig. 4 Physical images of hydrogels with three shapes (a). The effect of droplet fall height and ionic species in solution on prepared samples (b).

where, C_0 and C_t are the initial concentrations and the concentrations of MB at time t, respectively.

Fig. 5 shows the removal results of MB for GO-M prepared with different ion modulation. According to Fig. 5a, when the heights were the same, the samples prepared with different ion modulation showed obvious variations for MB removal, and the samples prepared with Ca^{2+} modulation showed a faster MB removal effect. It is hypothesized that the introduction of different ions has different effects on the internal structure and molding process of hydrogels. According to the SEM results in Fig. 2, the surfaces of GO-Ca prepared by Ca^{2+} modulation showed more folds, which could provide more reaction contact sites, thus improving the removal effect of MB. The poor MB removal effect of GO-Al may be due to the accumulation of GO in the crosslinking process of Al^{3+} (Fig. 2c), which reduces the reaction contact site.

However, the specific surface area of hydrogels tends to increase with the elevation of ionic valence as can be seen from Table 1. The specific surface area of Al^{3+} crosslinked hydrogels is the largest, but the adsorption capacity is weak. This may be related to the layer spacing, GO-Al has a large layer spacing and is filled with more water molecules. The results of Che-Ning Yeh *et al.* showed that the layer spacing of the Al^{3+} crosslinked membranes became larger after drying and rehydrating.[41] Our previous study also showed that the layer spacing of GO-Al membranes was larger than that of GO-Ca membranes.[42] Since hydrogels were used in this study, it is hypothesized that the pre-adsorption may involve the exchange of positions between water molecules and MB molecules and the occupation of reaction sites. Therefore, it will lead to the phenomenon that GO-Al hydrogels have large specific surface area but slow adsorption efficiency.

Further, we found that the removal of MB by GO-M-H (Fig. 5b) was significantly better than that of GO-M-L (Fig. 5a), and the conclusion is confirmed by the discolouration results of the MB solution in Fig. S2.† Comparison of Fig. S1b and c† shows that the N_2 adsorption of GO-Ca-H is larger than the N_2 adsorption of GO-Ca-L at higher relative air pressure, indicating that the adsorption capacity of GO-Ca-H is stronger. It may be attributed to the increase in specific surface area, and the results of Table 1 also showed the GO-M-H had a larger specific surface area than GO-M-L, and lager specific surface area provides more contact sites for reaction, thus enhancing removal effect of MB. Besides, the significant enhancement of MB removal by GO-K-H may be attributed to the fact that

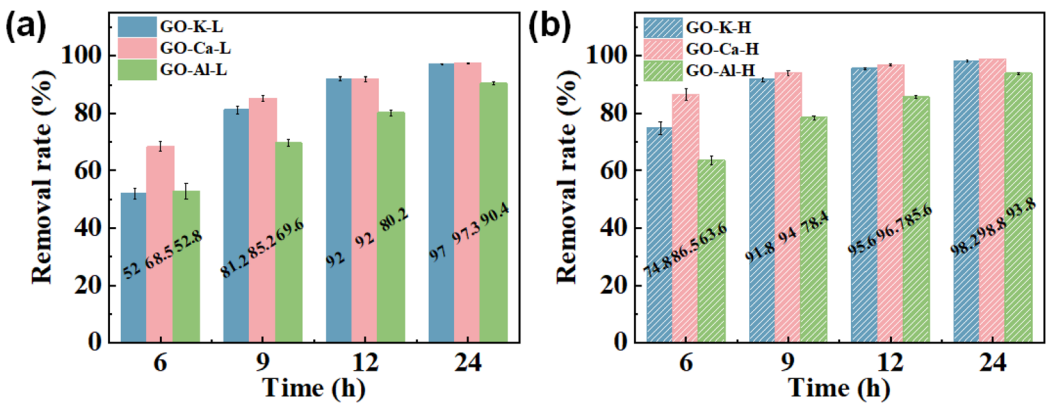

Fig. 5 Removal effect of MB based on GO-M-L (a) and GO-M-H (b). L indicates a preparation height of 0.5 cm and H indicates a preparation height of 3.5 cm (M: K, Ca, Al).

jellyfish-like samples have a larger specific surface area than bullet-like or cap-like samples.

3.4. Effect of solution pH on adsorption of MB

Fig. 6a–c show the removal of MB by the GO-M hydrogels at different pH values. The pH of the solution significantly influenced the MB removal efficiency of the adsorption process. As shown in Fig. 6a–c, the best removal of MB was achieved under neutral conditions, and both acidic and alkaline conditions were unfavourable for MB adsorption. MB is a cationic dye with a positive surface charge, which is more easily adsorbed when the adsorbent surface is negatively charged, which can be explained by the existence of electrostatic attraction between the two.[43] Carboxylic acid functional groups on the surface of the material under acidic conditions undergo protonation, which is detrimental to MB adsorption. Under alkaline conditions, positively charged sites may have been generated on the surface of the hydrogels, leading to electrostatic repulsion between these sites and the MB molecules, weakening the adsorption of MB. It can be seen that the pH of the solution affects the adsorption process.

3.5. Adsorption kinetic study

In order to explore the adsorption kinetics and investigate the relationship between the adsorption process and the contact time, 20 mL of MB solution (50 mg L^{-1}) was added to 10 mg of

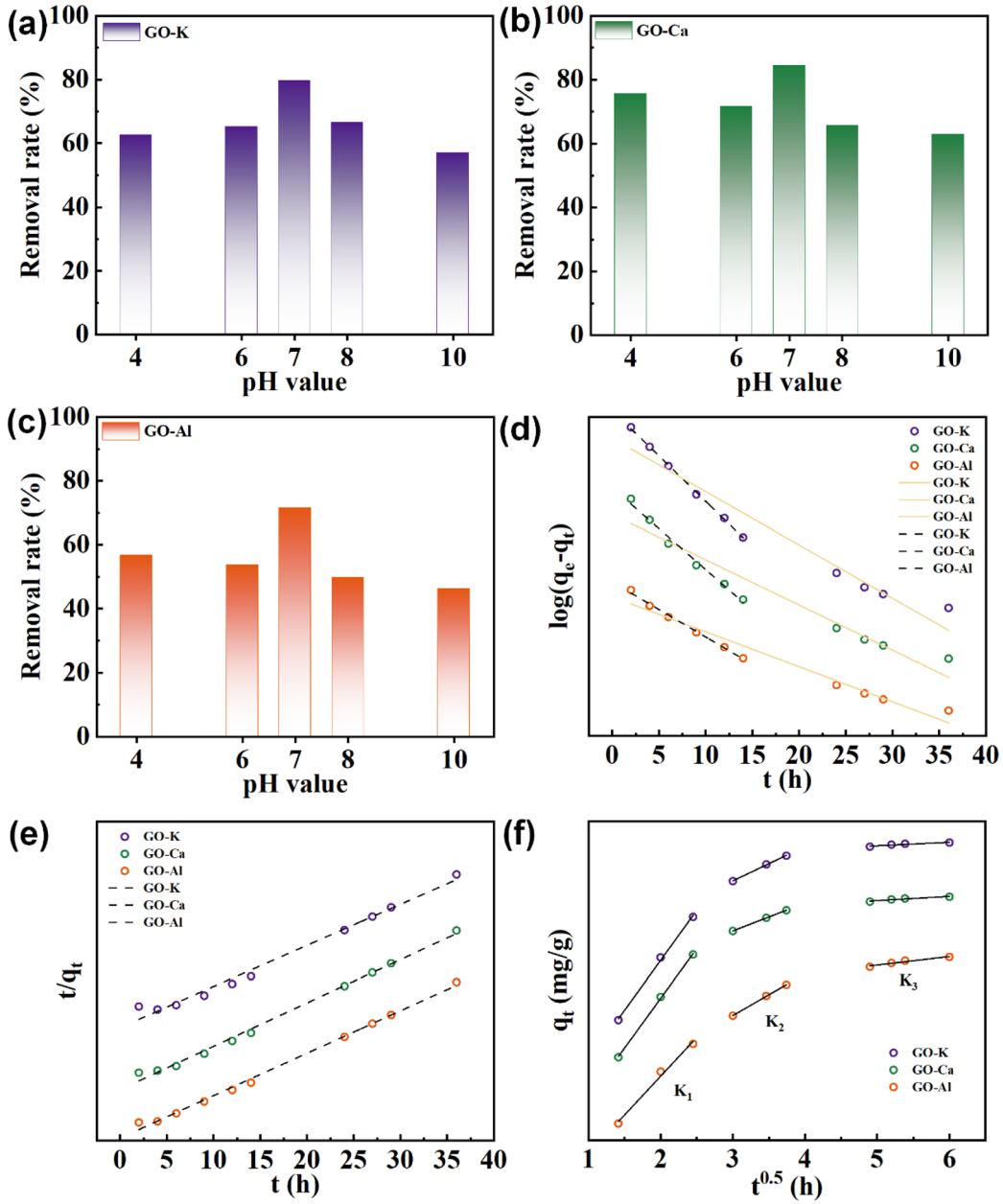

Fig. 6 Effect of solution pH on MB removal by GO-M hydrogels (data for the 12 h reaction of the adsorption system) (a–c). Pseudo-first-order model (d) and pseudo-second-order model (e) for GO-M adsorbed MB. Intraparticle diffusion model for GO-M (f) (M: K, Ca, Al).

Table 2 Absorption kinetic modeling correlation coefficients for MB adsorption on ion-modulated GO hydrogels

	Pseudo-first-order kinetic			Pseudo-second-order kinetic		Linear relation		
Absorbent	k_1 h^{-1}	$q_e{}^1$ mg g^{-1}	$R_1{}^2$	k_2 g (mg^{-1} h)	$q_e{}^2$ mg g^{-1}	$R_2{}^2$	$R_1{}^2$	$R_2{}^2$
GO-K	0.18	98.93	0.994	0.0017	117.22	0.973	0.937	0.984
GO-Ca	0.21	96.88	0.997	0.0023	111.92	0.981	0.921	0.994
GO-Al	0.16	93.04	0.998	0.0015	111.88	0.994	0.955	0.996

adsorbent, which was allowed to stand at room temperature for 36 h. The pseudo-primary and pseudo-secondary kinetic models were used to analyze and simulate the adsorption process, denoted as:[44]

$$\log(q_e - q_t) = \log q_e - \frac{k_1}{2.303}t \quad (2)$$

$$\frac{t}{q_t} = \frac{1}{k_2 q_e{}^2} + \frac{1}{q_e}t \quad (3)$$

where q_e (mg g^{-1}) is adsorption capacity at equilibrium. q_t (mg g^{-1}) is the adsorption capacity at time t (h). t (h) is the contact time, k_1 (h^{-1}) is the rate constant of pseudo-first-order model, k_2 (g (mg^{-1} h)) is the rate constant of pseudo-second-order model, respectively. Linear plots of $\log(q_e - q_t)$ *versus* contact time t and t/q_t *versus* contact time t were plotted as shown in Fig. 6d and e.

The fitted data are shown in Table 2, both the fitted primary kinetic model and the fitted secondary kinetic model have high R^2 values, but only the fitted secondary kinetic model fits well with the adsorption process after transforming into a linear model. The results indicate that the whole adsorption process is mainly influenced by the chemisorption mechanism.

In order to further explain the adsorption mechanism and the control steps of adsorption rate, the adsorption process was analyzed by using the intraparticle diffusion model, which was expressed as:[45]

$$q_t = Kt^{0.5} + C \quad (4)$$

where K (mg g^{-1} $h^{-0.5}$) is Weber–Morris rate constant, which represents intraparticle diffusion rate. C (mg g^{-1}) is the intercept which responses the thickness of adsorption boundary layer.

As shown in Fig. 6f, the entire adsorption process can be divided into three stages, including the initial stage of adsorption with a high slope, the mid-stage of adsorption with a significantly lower slope, and the equilibrium stage. Combined with Table 3, it can be seen that the K value of the first stage is the largest, the adsorption rate is faster, the adsorption mainly occurs on the outer surface, and the external diffusion is the main step limiting the adsorption rate. In the second stage, the adsorption rate decreases, and MB molecules diffuse into the interior of the adsorbent, causing a series of chemical adsorption, and the adsorption rate is mainly controlled by internal diffusion. The third stage has a lower K value and the adsorption process reaches equilibrium with a slow increase in adsorption. The results show that the multistage fitting results are more consistent with the actual adsorption process, and the whole adsorption process is controlled by both external and internal diffusion.

3.6. GO@MXene hydrogels

3.6.1. The stability of GO-M and GO@MXene-M hydrogels. Considering the excellent performance of MXene in removing MB,[46,47] GO@MXene hydrogels were prepared by combining GO materials with MXene materials, and their adsorption capacity was investigated. According to Fig. S4d–f,† the interior of the GO@MXene-M hydrogel exhibits an irregular porous structure. The insets of Fig. S4g–i and S5a† suggested that metal ions (K^+, Ca^{2+} and Al^{3+}) were able to be introduced into the prepared GO@MXene-M samples in this way. Fig. S5b† showed the survey scan of titanium (Ti) in GO@MXene-M, confirming the presence of MXene in the prepared GO@MXene-M samples.

Furthermore, the mechanical stability of different GO-M and GO@MXene-M hydrogels was studied in water, as shown in Fig. 7. It can be seen from Fig. 7a that the colour of the water in which the GO-Na hydrogels are immersed gradually turns yellow as the immersion time increases, which means that the GO-Na hydrogels decompose, and the results indicated GO-Na hydrogels had poorer stability compared to other GO-M hydrogels. It should be emphasised that increasing the concentration of Na ions also did not inhibit the decomposition of GO-Na hydrogels. Moreover, the results in Fig. 7 also showed the introduction of MXene could improve the stability of

Table 3 Parameters for modeling intraparticle diffusion for MB adsorption on ion-modulated GO hydrogels

	Stage I			Stage II			Stage III		
Absorbent	K_1	C_1	$R_1{}^2$	K_2	C_2	$R_2{}^2$	K_3	C_3	$R_3{}^2$
GO-K	42.39	−36.64	0.996	14.65	37.88	0.997	1.48	89.32	0.84
GO-Ca	42.1	−29.86	0.999	11.89	47.23	1	1.79	86.82	0.89
GO-Al	32.96	−22.38	0.98	17.67	16.24	0.98	3.64	72.41	0.93

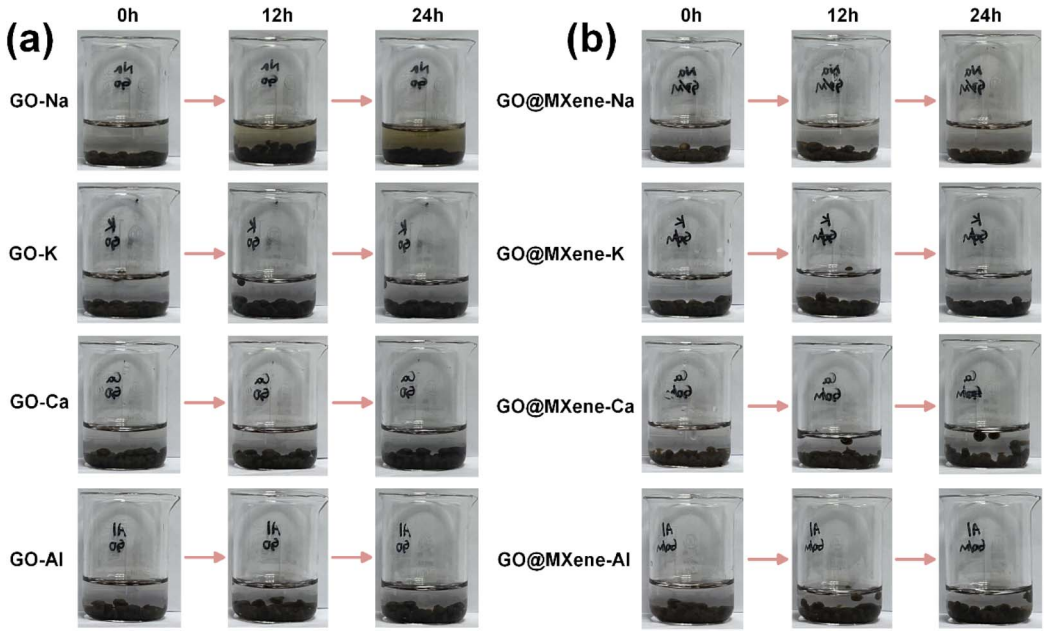

Fig. 7 The stability of GO-M (a) and GO@MXene-M (b) hydrogels in water (M: Na, K, Ca, Al).

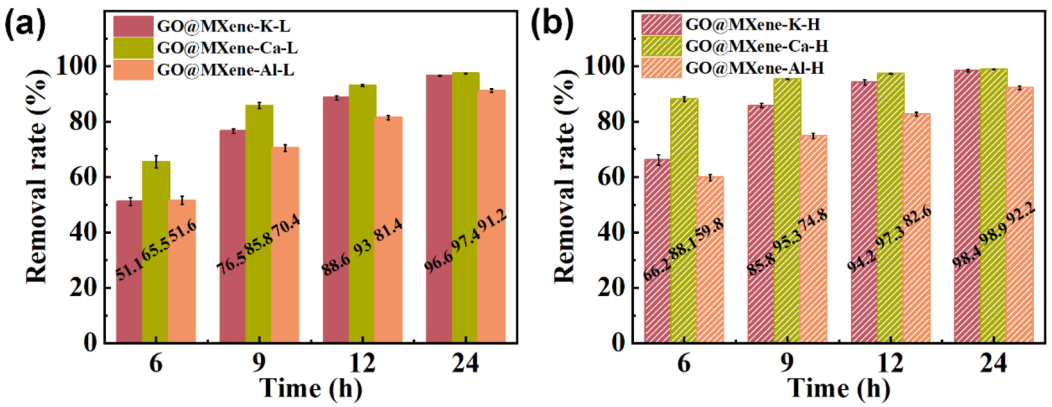

Fig. 8 Removal effect of MB based on GO@MXene-M-L (a) and GO@MXene-M-H (b). L indicates a preparation height of 0.5 cm and H indicates a preparation height of 3.5 cm (M: K, Ca, Al).

prepared hydrogels. In addition, our study also shows that GO@MXene hydrogels can be prepared without introducing metal ions, but their stability is also poor, as shown in Fig. S3.†

3.6.2. MB adsorption based on GO@MXene-M. Fig. 8a and b show the removal results of MB for GO@MXene-M-L and GO@MXene-M-H prepared with different ion modulation. As can be seen from Fig. 8a, GO@MXene-Ca hydrogels adsorbed MB more efficiently, although the specific surface area of GO@MXene-Al hydrogels was greater than that of GO@MXene-K and GO@MXene-Ca hydrogels (Table S1†). This may be due to the high roughness of the surface of GO@MXene-Ca hydrogels with more folds (Fig. S4†), which can provide more reaction sites. Comparing Fig. 8a and b, the removal rate of MB by GO@MXene-M-H hydrogels was higher than that of GO@MXene-M-L hydrogels. As shown in Fig. S1c and d,† the N_2 adsorption–desorption isotherms of the GO/MXene hydrogels also exhibit Type IV curves with H3-type hysteresis loops, while the hysteresis loop of GO/MXene-Ca-H is more pronounced, suggesting a possible expansion of interlayer spacing, thereby enhancing adsorption performance. Additionally, the N_2 adsorption capacity of GO@MXene-Ca-H was higher than that of GO@MXene-Ca-L, indicating stronger adsorption capability. This is hypothesized to result from morphological changes in the hydrogels, which influence their specific surface area (Table S1†).

Furthermore, the effects of solution pH and contact time on adsorption were also investigated. Fig. S6a–c† show the removal of MB by the GO@MXene-M hydrogels at different pH values. The results show that when the pH of the solution was increased from 4 to 10, only neutral conditions showed the best removal of methyl bromide, while both acidic and basic conditions were not favorable for the adsorption of methyl bromide. The

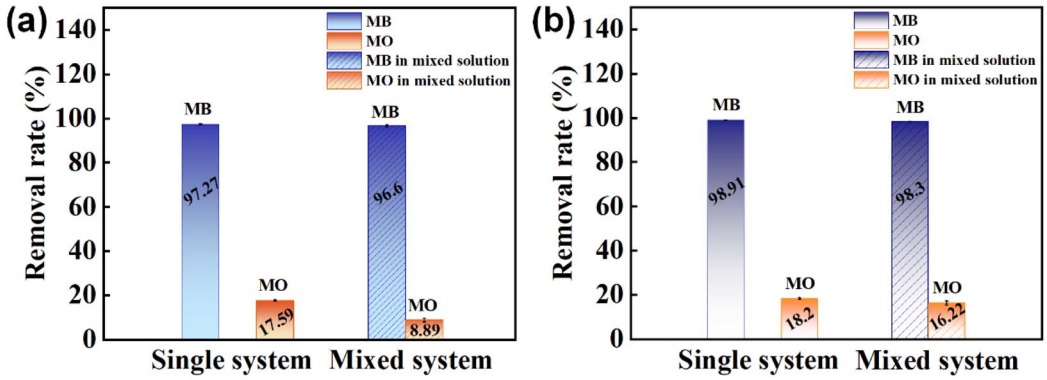

Fig. 9 Selective adsorption of GO-Ca-H (a) and GO@MXene-Ca-H (b).

kinetics results of the fitted GO@MXene-M-adsorbed MB are shown in Fig. S6d–f.† The fitted data are shown in Table S2,† the R^2 of the pseudo-first-order kinetics is larger than the R^2 of the pseudo-second-order kinetics, but after transforming into a linear model, ${R_2}^2$ is larger than ${R_1}^2$, which indicates that the adsorption process is more consistent with the proposed secondary kinetics model. The results of intraparticle diffusion showed that GO@MXene-M hydrogels also belong to the typical three-stage adsorption (Table S3†).

3.7. Selective adsorption

In order to evaluate the potential practical applications, selective adsorption experiments based on GO-Ca-H and GO@MXene-Ca-H hydrogels were performed. In this study, MO, an anionic dye widely used in the printing and dyeing industry, was used as a competing dye, and the selective adsorption properties of GO-Ca-H and GO@MXene-Ca-H in single and mixed dye solutions were investigated as shown in Fig. 9. According to the results of Fig. 9a, the removal rate of MB and MO by GO@MXene-Ca-H was respectively 98.91% and 18.2% in the single dye solution, and GO@MXene-Ca-H remained high removal rate of MB (98.3%) in a mixed system. Like GO@MXene-Ca-H, GO-Ca-H also showed good selective adsorption in single and mixed dye solution, as shown in Fig. 9b. Fig. S7† shows the discolouration results of MB and MO in single and mixed systems, which also identified that GO-Ca-H and GO@MXene-Ca-H have good selective adsorption for cationic dyes MB.

4. Conclusions

In summary, different ion modulated GO and GO@MXene hydrogels were prepared and investigated, and the introduction of different ions not only improve the stability of GO and GO@MXene hydrogels in solution, but also affect the adsorption property of GO and GO@MXene hydrogels on MB. Due to the change of specific surface area caused by morphology, GO and GO@MXene hydrogel prepared by Ca^{2+}-modulated showed better adsorption properties of MB than GO and GO@MXene hydrogel prepared by K^+ and Al^{3+} modulated. Besides, the height at which the droplets fall also leads to a change in the shape of the hydrogel, which in turn leads to a change in its specific surface area, and it also affects the removal effectiveness of the hydrogel on MB. And GO-M-H and GO-MXene-M-H showed better adsorption properties of MB than GO-M-L and GO-MXene-M-L. These different ions regulated hydrogels also have good selectivity and are expected to be adsorbents for the removal of cationic dyes from textile dye wastewater. The study of adsorption kinetics showed that the adsorption of MB by ion-modulated hydrogels was more in line with the pseudo-secondary kinetic model, and the results of intraparticle diffusion indicated that the whole adsorption process received dual control by both internal and external diffusion.

Data availability

All data included in this study are available upon request by contact with the corresponding author.

Conflicts of interest

The authors declare that they have no known competing financial interests or personal relationships that could have appeared to influence the work reported in this paper.

Acknowledgements

This work was supported by the Research Initiation Program for Specially Appointed Professors of Xinxiang Medical College [505526], the Key Scientific Research Items of Henan Province Colleges and Universities [22A416001].

References

1 P. Zhu, Y. Deng and C. Wang, *Carbohydr. Polym.*, 2017, **174**, 804–811.
2 M. Zou, J. Sun and Z. Xiang, *Adv. Healthcare Mater.*, 2021, **10**(6), DOI: **10.1002/adhm.202001502**.
3 X. Zhang, D. Liu, L. Yang, L. Zhou and T. You, *J. Mater. Chem. A*, 2015, **3**, 10031–10037.
4 Q. Zhao, X. Zhu and B. Chen, *Chem. Eng. J.*, 2018, **334**, 1119–1127.

5 J. S. da Costa, E. G. Bertizzolo, D. Bianchini and A. R. Fajardo, *J. Hazard. Mater.*, 2021, **418**, 126405.
6 Y. Zhang, S. Gong, Q. Zhang, P. Ming, S. Wan, J. Peng, L. Jiang and Q. Cheng, *ChemInform*, 2016, **47**(25), DOI: 10.1002/chin.201625226.
7 R. Narayan, J. E. Kim, J. Y. Kim, K. E. Lee and S. O. Kim, *Adv. Mater.*, 2016, **28**, 3045–3068.
8 W. Peng, H. Li, Y. Liu and S. Song, *J. Mol. Liq.*, 2016, **221**, 82–87.
9 Y. Wang, M. Wu, J. Wang, J. Huang, K. Yang, X. Miao and L. Zhang, *Mater. Today Commun.*, 2024, **39**, 108676.
10 Y. Xu, K. Sheng, C. Li and G. Shi, *ACS Nano*, 2010, **4**, 4324–4330.
11 H. Bai, C. Li, X. Wang and G. Shi, *Chem. Commun.*, 2010, **46**, 2376.
12 M. A. Worsley, P. J. Pauzauskie, T. Y. Olson, J. Biener, J. H. Satcher and T. F. Baumann, *J. Am. Chem. Soc.*, 2010, **132**, 14067–14069.
13 Y.-T. Zhuang, R. Jiang, D.-F. Wu, Y.-L. Yu and J.-H. Wang, *J. Colloid Interface Sci.*, 2019, **540**, 572–578.
14 Q. Wang, J. Shao, J. Xu, F. Dong, Y. Xiong and Q. Chen, *J. Colloid Interface Sci.*, 2022, **607**, 253–268.
15 Y. Fan, W. Ma, D. Han, S. Gan, X. Dong and L. Niu, *Adv. Mater.*, 2015, **27**, 3767–3773.
16 N. Ormategui, A. Veloso, G. P. Leal, S. Rodriguez-Couto and R. Tomovska, *ACS Appl. Mater. Interfaces*, 2015, **7**, 14104–14112.
17 H. Huang, M. Yan, C. Yang, H. He, Q. Jiang, L. Yang, Z. Lu, Z. Sun, X. Xu, Y. Bando and Y. Yamauchi, *Adv. Mater.*, 2019, **31**(48), DOI: 10.1002/adma.201903415.
18 Y. Yin, X. Li, H. Ma, J. Zhang, D. Yu, R. Zhao, S. Yu, G. Nie and H. Wang, *Nano Lett.*, 2021, **21**, 2224–2231.
19 K. Zhihui and D. Min, *ACS Biomater. Sci. Eng.*, 2022, **8**, 2849–2857.
20 N. Li, Q. Ma, L. Xu, Y. Wang, L. Zhang, Y. Jiang and H. Liu, *Mater. Today Commun.*, 2024, **39**, 109319.
21 C. Qi, C. Luo, Y. Tao, W. Lv, C. Zhang, Y. Deng, H. Li, J. Han, G. Ling and Q.-H. Yang, *Sci. China Mater.*, 2020, **63**, 1870–1877.
22 Z. J. Huang, X. liang Lu, H. Z. Chi, W. Zhang, Q. Xiong and H. Qin, *Chemelectrochem*, 2021, **8**, 3962–3970.
23 Y. Zhang, L. Zhang, G. Zhang and H. Li, *ACS Appl. Mater. Interfaces*, 2018, **10**, 21565–21572.
24 Q. Meng, C. Du, Z. Xu, J. Nie, M. Hong, X. Zhang and J. Chen, *Chem. Eng. J.*, 2020, **393**, 124684.
25 Z. Zhang, Q. Dou, S. Wang, D. Hu, X. Guo, B. Liao, Z. Zhao, H. Liu and Q. Dai, *J. Mater. Chem. C*, 2020, **8**, 9655–9662.
26 B. Tan, H. Zhao, L. Du, X. Gan and X. Quan, *Biosens. Bioelectron.*, 2016, **83**, 267–273.
27 W. Cheng, Y. Chen, L. Teng, B. Lu, L. Ren and Y. Wang, *J. Colloid Interface Sci.*, 2018, **513**, 314–323.
28 Y. Zhang, M. Qin, C. Xing, C. Zhao, X. Dou and C. Feng, *ACS Nano*, 2020, **14**, 17151–17162.
29 Y. Piao and B. Chen, *Int. J. Biol. Macromol.*, 2017, **101**, 791–798.
30 X. Zhao, W. Yao, W. Gao, H. Chen and C. Gao, *Adv. Mater.*, 2017, **29**(35), DOI: 10.1002/adma.201701482.
31 L. Xu, L. Cui, M. Jia, Y. Li, J. Gao and X. Jin, *Carbohydr. Polym.*, 2018, **195**, 593–600.
32 M. Fayazi and M. Ghanei-Motlagh, *J. Colloid Interface Sci.*, 2021, **604**, 517–525.
33 W. Jiang, S. Wang, X. Yan, F. Lin, Z. Li, X. Fan, W. Ren, G. Zhao and Y. Yu, *Mater. Chem. Phys.*, 2023, **294**, 127067.
34 M. Fayazi and E. Rezvannejad, *Inorg. Chem. Commun.*, 2024, **159**, 111786.
35 S. Eslaminejad, R. Rahimi and M. Fayazi, *J. Taiwan Inst. Chem. Eng.*, 2023, **152**, 105181.
36 K. Chaturvedi, V. Hada, S. Paul, B. Sarma, D. Malvi, M. Dhangar, H. Bajpai, A. Singhwane, A. K. Srivastava and S. Verma, *Top. Curr. Chem.*, 2023, **381**, 11.
37 N. My Tran, Q. Thanh Hoai Ta, A. Sreedhar and J.-S. Noh, *Appl. Surf. Sci.*, 2021, **537**, 148006.
38 K.-N. Zhang, C.-Z. Wang, Q.-F. Lu and M.-H. Chen, *Int. J. Biol. Macromol.*, 2022, **209**, 680–691.
39 L. Ai, C. Zhang and Z. Chen, *J. Hazard. Mater.*, 2011, **192**, 1515–1524.
40 L. Zhang, D. Huang, P. Zhao, G. Yue, L. Yang and W. Dan, *Sep. Purif. Technol.*, 2022, **288**, 120718.
41 C.-N. Yeh, K. Raidongia, J. Shao, Q.-H. Yang and J. Huang, *Nat. Chem.*, 2015, **7**, 166–170.
42 W. Jiang, X. Chen, X. Yan, J. Li, L. Xie and Y. Yu, *Colloids Surf., A*, 2024, **702**, 135098.
43 B.-M. Jun, J. Heo, N. Taheri-Qazvini, C. M. Park and Y. Yoon, *Ceram. Int.*, 2020, **46**, 2960–2968.
44 Z.-H. Zhang, J.-Y. Xu and X.-L. Yang, *Mater. Chem. Phys.*, 2021, **260**, 124123.
45 J. Hoslett, H. Ghazal, N. Mohamad and H. Jouhara, *Sci. Total Environ.*, 2020, **714**, 136832.
46 C. Hao, G. Li, G. Wang, W. Chen and S. Wang, *Colloids Surf., A*, 2022, **632**, 127730.
47 J. Qu, D. Teng, X. Zhang, Q. Yang, P. Li and Y. Cao, *Ceram. Int.*, 2022, **48**, 14451–14459.